Variations of the three-dimensional structure of the *Escherichia coli* ribosome in the range of overlap views

An application of the methods of multicone and local single-cone three-dimensional reconstruction

Jose María Carazo, Terence Wagenknecht, and Joachim Frank
Wadsworth Center for Laboratories and Research, New York State Health Department, Albany, New York 12202-0509

ABSTRACT Electron microscopic techniques are among the most important tools for obtaining structural information of biological specimens. However, the three-dimensional (3D) structural analysis of asymmetrical specimens that do not form crystalline sheets has traditionally presented serious methodological obstacles to its accomplishment. One of the fundamental questions to be addressed in this type of structural study is in what way, and to what degree, does the 3D structural conformation depend on the orientation of the specimen with respect to the electron microscopic support films. As a step in studying this problem, we have analyzed the variations of the 3D structure of the *Escherichia coli* 70S monosome by performing four different 3D reconstructions of the 70S monosome from subsets of images in the so-called overlap range of views. These subsets were selected according to a multivariate statistical analysis performed on the total population of overlap-range specimen images. A certain amount of structural variability exists among the 3D reconstructions, although many of the main morphological characteristics, as the relative orientation between the ribosomal subunits, remain unchanged. We have also generalized the random conical reconstruction technique (Radermacher, M., T. Wagenknecht, A. Verschoor, and J. Frank. 1987. *J. Microsc.* 146:113–136) to include those cases where the specimen exhibits a rocking behavior with respect to the support. The resulting Multicone Reconstruction Technique has been applied to computer-generated images as well as the *E. coli* 70S monosome images from part of the overlap range of views.

INTRODUCTION

Structural analysis has proven to be a powerful tool in the elucidation of the functions carried out by many biological systems. Electron microscopy has been a key technique for these structural studies, since it provides information in the form of images that can, in many cases, be easily related to properties of the specimen structure. However, when a detailed structural analysis is needed, a fundamental limitation of this kind of images immediately appears: they only represent two-dimensional (2D) projections of the real three-dimensional (3D) structure of the specimen onto a plane perpendicular to the electron beam. To quantitatively describe the specimen's 3D structure, such projection images need to be combined. A number of quite different techniques have been developed to treat this problem of 3D reconstruction in electron microscopy (see Crowther et al., 1970; Henderson and Unwin, 1975; Radermacher, 1988).

Most of these techniques are applicable only to either 2D crystals or specimens having a high degree of symmetry. Recently, however, some techniques for 3D reconstruction of asymmetrical, non-crystalline specimens imaged by low doses of electrons have been proposed (Provencher and Vogel, 1983; Vainshtein and Goncharov, 1986; Radermacher et al., 1987*a*; van Heel, 1987). In principle, these techniques open the possibility of studying the broad range of specimens that neither present high degrees of structural symmetries nor form 2D crystals. One of these techniques, the random-conical tilt-series method (Radermacher et al., 1987*a*), has already been applied to a number of ribosome specimens, both prokaryote (Radermacher et al., 1987*b*; Carazo et al., 1988; Wagenknecht et al., 1988) and eukaryote (Zhang et al., 1987; Verschoor, A. and J. Frank, manuscript submitted for publication), resulting in detailed models of their 3D structures.

Inherent to all these techniques is the assumption that the specimen's structure retains important information about the native state, both after interaction with the specimen-support films and after irradiation with electrons. The way in which these two factors can influence the final results depends on the method used. For a 3D reconstruction from a 2D crystal the number of exposures that are taken from the same field varies among different studies, usually being ~10, although a few studies have been carried out with only one exposure per field. For the 3D reconstruction from single particles the method developed by Radermacher et al. (1987*a*) is optimum from the standpoint of radiation damage to the specimen (only one image, at a high tilt angle, is needed). However, it assumes that the interaction between individual particles and the support films, which results in a given view, does not destroy or severely degrade the specimen structure.

In this work we will, using the *E. coli* 70S monosome in the O-R range of overlap views (Verschoor et al., 1986) as

a model system, focus on the possible structural modifications that individual specimens can undergo when interacting with the electron microscopic support films. We will prove that some structural changes do occur depending on the precise way in which the 70S monosome interacts with the support films, but that very important morphological features, such as the relative orientation between the ribosomal subunits, are still preserved in the whole range of views. In addition, we will present a generalization of Radermacher et al.'s (1987*a*) 3D reconstruction method—which requires the specimen to lie on the support films in a well defined orientation—to those cases in which the specimen assumes an entire range of different orientations but does not change its structure significantly. We call this generalization the Multicone 3D Reconstruction Method. We will give evidence for its efficiency in compensating for orientational differences using computer-simulated data as well as experimental data coming from part of the range of 70S monosome views considered.

IMAGE PROCESSING METHODS

Overview

The techniques used in this work to perform the 3D reconstruction procedure are based on the random-conical-tilt-series method (Frank et al., 1978; Radermacher et al., 1987*a*). In essence, this method starts from a pair of micrographs showing the same field both at a high tilt angle and without tilt. The tilted-field image is obtained first. Only tilted-specimen images selected from this field enter the 3D reconstruction. The untilted-specimen images are used to obtain the parameters necessary to completely specify the conical data collection geometry. They are here additionally analyzed by multivariate statistical analysis (MSA) methods so as to identify subsets of particles that show the same appearance (indicative of the same "rocking position") on the specimen support before 3D reconstruction (Carazo et al., 1988*b*).

Alignment and multivariate statistical analysis

Untilted images presenting the specimen in a range of view are rotationally and translationally aligned with respect to a common reference (Frank et al., 1978, 1981). MSA, specifically, correspondence analysis of the type described by van Heel and Frank (1981) and Frank and van Heel (1982) is performed on the resulting aligned set of images. This analysis provides a quantitative breakdown of the image population according to the different patterns of variability. We usually call these patterns "factors," although the name eigenimages (Bretaudiere and Frank, 1986) is also appropriate.

Global reconstruction and co-projection studies

In the case of the *E. coli* 70S monosome occurring in the O-R range of overlap views, a specific MSA factor has been shown to discriminate according to change of orientation of the specimen on the support films. However, the observations leading to this conclusion are rather qualitative, and fail to establish a calibration of the angular range.

In an attempt to overcome this problem, we use the following strategy: (a) Obtain a preliminary reconstruction from a large subset of the projections, eliminating particles that deviate by a certain margin from the average. We term this the global reconstruction. (b) Compute a series of projections that show the global reconstruction rotated around the putative rocking axis, in an angular range sufficiently large to cover the expected experimental range. (c) Compare these calculated projections with the experimental projections (or small averages thereof in factor space) in order to obtain matching pairs. (d) On the basis of this matching, calibrate the orientation-related factor.

Apart from a calibration of the angular range, our strategy provides a test of both the qualitative identification of a factor as being orientation-related and the hypothesis that most of the observed projections arise from the same, essentially unchanged structure. The ability to predict experimental projections that have not been used in obtaining the global reconstruction constitutes a very convincing proof of validity of the model and internal consistency of the analysis.

Technically, the comparison of calculated with experimental projections in step (*c*) above is done by a so-called co-projection of the calculated projection images into the space spanned by MSA of the experimental projections. (Note that here the term projection is used with two different meanings: in one meaning, it is the process by which the 2D appearance of a 3D structure is generated by summation along specified directions; in the other meaning [i.e., in co-projection], it is the formation of a scalar product which determines the place of an image [which in this case happens to be a projection in the former sense] in factor space.) In conjunction with the co-projection analysis, we speak of the images from which the MSA factors are calculated as "active images" and those merely co-projected as "inactive."

Multicone tilt-series formulation

If a set of untilted projection images can be interpreted as the result of rocking of the specimen around a given axis

on the support plane and the rocking angle is known, then their corresponding tilted projection images can be incorporated into a single 3D reconstruction. The data collection geometry is now called multicone, since the projection images can be geometrically described as a set of conical tilt series belonging to different cones (Fig. 1). Each cone is formed by images coming from a specimen that is tilted (rocked) by the same angle β with respect to the 3D reference orientation. The parameters specifying each conical tilt series are the cone half-angle θ, given by the inclination of the specimen grid, and the azimuthal (in-plane) ϕ angle of each projection image in the coordinate system of the particle in its first (reference) orientation. The problem is now how to merge elements from different cones into a single reconstruction. It is shown in the formulas below how both the tilt angle, θ', and the azimuthal angle, ϕ', for particles not in the reference cone, may be expressed in terms of the coordinate system defined by the reference cone. In addition, a new term, Ω', is needed, which describes the orientation of the image in the new projection plane.

$$\phi' = \arctan\left(\frac{\sin\phi \sin\theta}{\cos\phi \cos\beta \sin\theta - \cos\theta + \sin\beta}\right) \quad (1)$$

$$\theta' = 90° - \arcsin(\sin\beta \sin\theta \cos\phi + \cos\beta \cos\theta) \quad (2)$$

$$\Omega' = \text{sign}(\sin\beta \sin\phi) \cdot [\sin^2\beta \sin^2\phi + (\sin\phi' \cos\phi - \cos\phi' \cos\beta \sin\phi)^2]^{1/2} \quad (3)$$

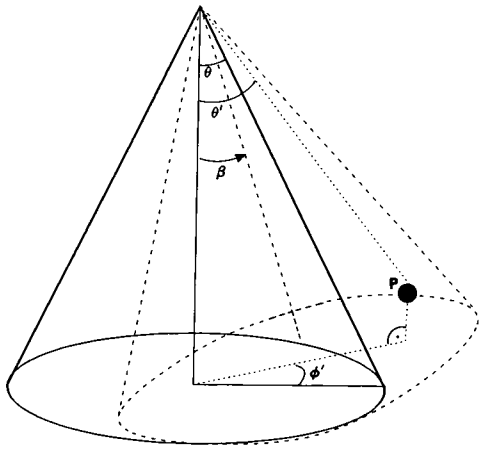

FIGURE 1 Geometry of merged conical-projection data set. Each circle represents the possible directions of view of a conical projection set (cone halfangle θ) with respect to the molecule. The two different cones are due to different orientations of the specimen on the electron microscopy support grid. We are expressing the direction of view of a projection P (original azimuth ϕ) by the new angles ϕ' and θ'. (The additional rotation by Ω' in the projection plane cannot be shown in this figure.) (From Frank et al., 1988*b*, reproduced with permission by Wissenschaftliche Verlogsgesellschaft).

These formulas have been obtained using simple analytic geometry principles that can be found in most textbooks (see, for example, Eccles et al., 1982). They were derived in reciprocal space, making use of the central section theorem (Crowther et al., 1970), which states that the Fourier transform of a projection lies within a plane through the origin of the 3D Fourier transform of the object from which the projection image was formed. The ideas used in the derivation of the formulas were as follows.

In the coordinate system that we have used in this work, axes x and y define the specimen support plane, while axis z is parallel to the direction of the electron beam. Axis y always runs vertically in the figures presented here and axis x horizontally. First we calculate two vectors defining the image plane in reciprocal space, one being an in-plane vector and the other a vector normal to that plane. These two vectors are then rotated around the y^* axis by the negative rocking angle β (for simplicity we are considering the y^* axis as the rocking axis), and their new coordinates are obtained in the initial coordinate system. A vector within the rotated plane that intersects the x^*-y^* plane is found; its orientation is directly the desired new in-plane ϕ' angle. The new tilt angle θ' is derived from the coordinates of the vector normal to the rotated plane. The additional in-plane rotation Ω' that is necessary to apply to the projection images is due to the fact that the Fourier transform of a projection image has a given orientation within a plane in reciprocal space which changes with the overall rotation of the coordinate system.

It is now easy to generalize these formulas and apply them to the case where the orientation angles form a continuum, and the two cones are replaced by a continuum of cones. In summary, the formulas (1–3) allow conical-tilt projections of particles that lie in a given range of orientations on their support plane to be used in a single 3D reconstruction, provided that their orientations are known, and provided that they represent the specimen structure virtually unchanged. This method, which constitutes a generalization of the method proposed by Radermacher et al. (1987*a*), is termed the multicone 3D reconstruction method (Frank et al., 1988*b*).

RESULTS

1. Determination of the rocking behavior of the specimen

1.1 Co-projection studies

The O-R range of overlap views of the *E. coli* 70S monosome was previously shown by Verschoor et al. (1986) to qualitatively originate from the rotation of the 70S monosome around a single axis on the specimen support plane, which we usually refer to as the "rocking"

axis. In their study, Verschoor et al. (1986) found the first factor resulting from MSA of these views to be related to such a rotation. Also, this first factor accounts for a significant high percentage of the interparticle variance (13% compared with 5% for the second factor); it may thus inherently possess an important discriminatory power.

In a first attempt to quantitatively assess this rotational behavior, we calculated an initial global 3D reconstruction (see Wagenknecht et al., 1988) from those tilted images which corresponded to the untilted particles lying within $\pm 1\sigma$ from the mean image along factor 1. We then calculated a set of projection images ("calculated projections") from this global 3D reconstruction which were obtained by rotating the particle by $-35°$ to $+35°$ around the rocking axis determined by Verschoor et al. (1986). The calculated projections were then co-projected onto the factor map defined by the experimental views (Fig. 2) as described in Image Processing Methods. We found it especially useful to display the results of the co-projection study by showing a map of factor 1 versus factor 5 (Fig. 2). This is so because factor 1 is related to the rocking axis identified by Verschoor et al. (1986) and factor 5 has the effect of clearly separating the co-projection of calculated images having very similar coordinates along factor 1. Factor 5 may be related to rocking of the particle around a second axis.

If the first factor from MSA of these experimental views indeed represented a pattern of variation resulting exclusively from rocking of the particle in the range of overlap views, and if the specimen structure did not substantially change in the course of this rocking, then we would expect the calculated projections to co-project along a path following the direction of factor 1.

We were most interested in the behavior of the calculated projections lying outside of the data range used for the global 3D reconstruction; their positions on the factor map would indicate to what extent the appearance of rocked particles can be predicted from a model that has been obtained assuming no structural or orientational changes. In fact, we obtained quite a good agreement for the pathway followed by the calculated projections for rotation angles from $-35°$ to $\sim 0°$ which lay on the "O" (left) side of the map along the factor 1 direction (Fig. 2). However the pathway did not extend to the R side of the map (right-hand side of Fig. 2). The calculated projections for rocking angles between $\sim 0°$ and $+35°$ all had very similar coordinates along factor one, with no experimental projections located more than $+0.5\sigma$ away from the factor origin. Thus, the co-projection study identified a data range, encompassing most of the R-type images, which could not be explained as projections of the global model.

Another indicator for this discrepancy came from a study of the eigenimages (Bretaudiere and Frank, 1986) associated with factor 1. If the variations in the view's appearance were due solely to a change in the orientation of the 70S monosome with respect to the support films,

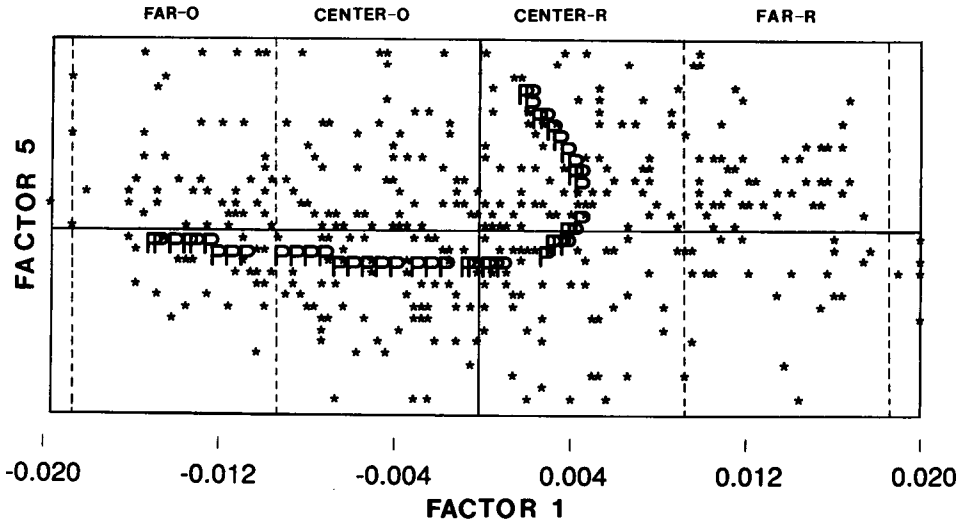

FIGURE 2 Correspondence analysis map (factors 1 versus 5) of 70S monosome untilted projections. Each experimental image is represented by an asterisk. In addition, projections of the initial global 3D reconstruction from the central region in factor 1 were generated in the range $-35°$ to $+35°$ and inactively "co-projected" onto the factor map (P). The division along factor 1 into four different regions is also indicated; the scale on this factor axis is shown in standard deviations of variance along the factorial axis (the total range shown along both factors is 4σ). On the left of the map are regions far-O and center-O, while on the right there are regions center-R and far-R.

then a close match would be observed between the factor-1 eigenimage from MSA of the experimental views and the corresponding eigenimages from MSA of the calculated projections alone. This is so because the calculated images were exclusively rocking related and factor 1 from MSA of these images accounted for most of the image variation (71%). Although the eigenimages (Fig. 3 *A* and *B*) do possess a close similarity in many important features, there are distinct differences, notably in the region corresponding to the L7/L12 stalk (*S* in Fig. 3) and in the region directly opposite to it. There is a strong density maximum in the stalk region in the eigenimage corresponding to the positive direction of factor 1 from MSA of the calculated projections that does not have a counterpart in the MSA of the experimental views. Also, a density change from maximum to minimum in the region opposite to the stalk for eigenimages of factor 1 in the MSA of the calculated projections is not found in the MSA of the experimental views.

We therefore find that factor 1 of the MSA of the experimental views is describing a more complex effect than rocking of an essentially unchanged structure. A more direct description of these effects requires a separate study of particles falling into different regions of the factor map along factor 1. We term a reconstruction that is done from a subset of projections, falling into a selected region in factor space, a "local reconstruction."

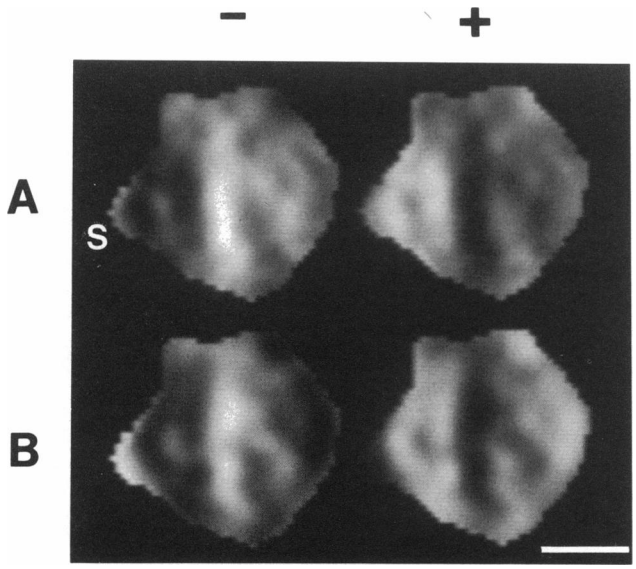

FIGURE 3 Factor-1 eigenimages resulting from the multivariate statistical analysis of (*A*) the total set of images of the O-R range of *E. coli* 70S monosome overlap views, (*B*) the set of projection images computed from the initial global 3D structure of the 70S monosome, simulating a rocking of the specimen from −35° to +35° as described in the main text. The signs on top of each column indicate images from either the negative (−) or positive (+) sides of the factor. *S*, L7/L12 stalk region. Bar, 10 nm.

1.2 Local 3D reconstructions and structural heterogeneity

To unambiguously analyze the extent of the rocking effect and the structural variations that the specimen exhibits, we divided the data set into four regions according to the images' coordinates along factor 1. The region termed far-O was formed by images lying between -1.8σ and -0.9σ along factor 1 (in our analysis the factor space origin is the site of the mean image); region center-O ranged from -0.9σ to 0; region center-R from 0 to 0.9σ; and region far-R from 0.9σ to 1.8σ (see Fig. 2). The numbers of images for these regions were, respectively, 79, 95, 79, and 84. Incidentaly, this division into four groups is similar to the one proposed by Frank et al. (1988*a*) in their analysis of this range of views by a combination of dynamic-clouds clustering and hierarchical ascendent classification methods. The far-O and far-R groups correspond to the two peripheral classes of Frank et al., while the two central groups jointly correspond to the central class in that study. Regions far-O and center-O will be collectively termed the O-subrange of views, while regions center-R and far-R will be termed the R-subrange of views.

Images within each of these four regions were analyzed separately. A local average was obtained from each region (Fig. 4) and the untilted images were rotationally and translationally realigned with respect to this new regional average. Their corresponding tilted images were then centered as described by Carazo et al. (1988) and used to calculate an independent 3D reconstruction for each region. All four reconstructions were low-pass filtered to 4.5 nm by a Fermi-type spatial-frequency filter as described by Frank et al. (1985). This frequency radius was derived from the 4 nm theoretical resolution limit for a conical data collection geometry with an average angular spacing of 15°, as obtained from the equations developed by Radermacher (1980). The structures were then studied with the help of solid-body surface representation techniques of the type described by Radermacher and Frank (1984). Surface views of these four reconstructions are shown in Fig. 5.

The far-O (Fig. 5 *A*) and the center-O (Fig. 5 *B*) reconstructions proved to be most closely matched. We were able to align the structures by using a 3D correlation algorithm (Carazo and Frank, 1988) and obtained an angle of +16° around an axis that was found to virtually coincide with the rocking axis previously proposed by Verschoor et al. (1986). Fig. 6 shows three slices spaced 1-nm apart through both of the 3D reconstructions after this 3D alignment. It is obvious that the aligned struc-

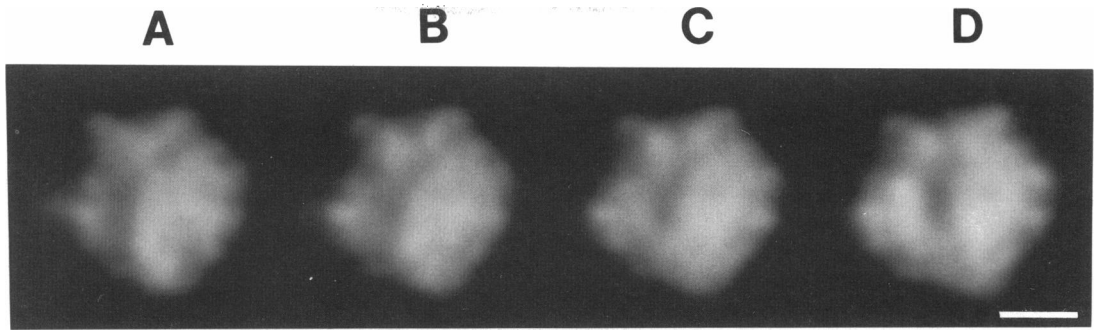

FIGURE 4 Local averages (filtered to 3.5 nm) of untilted 70S view from the four different regions indicated in Fig. 2. (*A*) far-O, (*B*) center-O, (*C*) center-R, and (*D*) far-R. The number of particles in each region is, respectively, 79, 95, 79, and 84. Bar, 10 nm.

tures obtained are very similar, although there are variations mainly in the region of the L7/L12 stalk. In fact, a 45° differential phase-residual analysis (Frank et al., 1981) performed on corresponding slices gave an average cross-resolution in the range of 4.5 to 5.0 nm.

The center-O and center-R reconstructions are still quite similar (Fig. 5 *B* and *C*), except for a change in the region at the base of the L7/L12 stalk and in the orientation of the stalk itself. The dimensions of the exposed interface canyon (a pronounced groove in the 50S subunit running from the L7/L12 stalk base to the L1 region; see Radermacher et al. [1987*b*]) slightly decrease in the center-R reconstruction as a result of this modification, and the stalk is angled off in a different way, turning more towards the observer in the center-R reconstruction than in the center-O (Fig. 5 *B* and *C*, 270° rotation). As before, we were able to match the center-R reconstruction to the center-O one by a further rotation of ~6° around the same axis that related the far-O and center-O reconstructions. However, this matching was less precise, as deduced from the much broader peak profile for the cross-correlation coefficients (results not shown), than the one performed between the reconstructions obtained from the O-subrange of views.

The far-R reconstruction, on the other hand, presents a structure that has a lower apparent resolution than any of the other local reconstructions (Fig. 5 *D*). The contours of this particle are smoother and the tip of the stalk is not well resolved. Also, there is a pronounced groove through this structure going from the part of the interface canyon closest to the head of the 50S subunit to the area located between the 50S head and the L1 region (Fig. 5, 0° rotation). When this 3D reconstruction was visualized from a direction parallel to the support film (Fig. 5 *D*, 90° and 270° rotation), it became clear that a second type of rocking was present, this time around an axis joining the base of the L7/L12 stalk with the L1 region and, thus, roughly perpendicular to the one previously identified in our study of the O-subrange of views. This second rocking was found to span an angular range of ~15°.

2. Multicone three-dimensional reconstruction

To analyze the possible degradation effects introduced into the computed 3D reconstructions as the result of an uncorrected rocking, and to determine the extent to which these effects could be compensated for by the multicone approach, we first studied a computer-simulated object.

2.1 Results with a computer-simulated object

The computer-generated test object used to evaluate the performance of the multicone 3D reconstruction method consisted of a 64 × 64 × 64 cube into which a set of ten hollow spheres with their centers lying in three different planes were placed. The inner and outer radii of the spheres were 2 pixels and 6 pixels, respectively. Three spheres were on plane 18 forming a triangle, four on plane 33 forming a square and the remaining three on plane 48 forming a straight line (see Fig. 7 *A*). The object formed by this set of spheres was then tilted around the y axis to simulate the rocking behavior of a real EM specimen. The rocking angles considered were $-20°$, $-10°$, $0°$, $+10°$, $+20°$. For each one of the rocking angles 12 projection images were calculated with $\Delta\phi = 30°$ and $\theta = 50°$. For a given rocking angle its associated projection images formed a conical tilt series. Thus, a multicone data-collection geometry was effectively generated (see Fig. 1).

Fig. 7 shows three sections through the original test object (Fig. 7 *a*), through its 3D reconstruction calculated under the (incorrect) assumption that the images formed a single-cone geometry (Fig. 7 *b*), and through the multicone 3D reconstruction of the object (Fig. 7 *c*). In this latter reconstruction the in-plane orientation angle

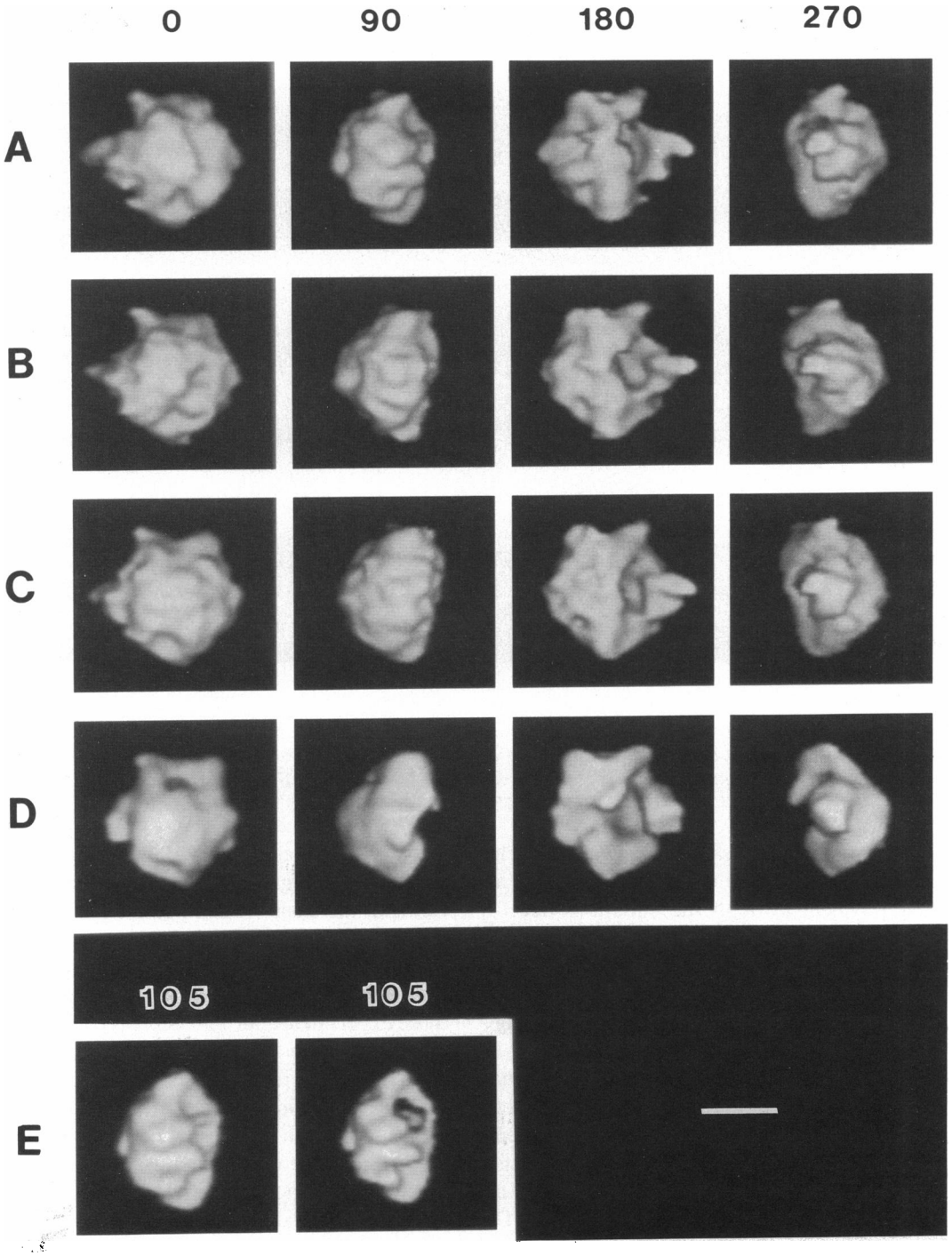

FIGURE 5 Surface representation of different local 3D reconstructions of the *E. coli* 70S monosome obtained from the four regions of the factor map shown in Fig. 2. The numbers 0°, 90°, 180°, 270° on top of the figure refer to the directions which were used to present the reconstructions *A–D*, in terms of a rotation in degrees around the vertical (*y*) axis. (*A–D*) Surface representation of the 3D reconstruction from (*A*) the far-O region, (*B*) the center-O region, (*C*) the center-R region, and (*D*) the far-R region. (*E*) Surface representation of the far-O reconstruction shown in (*A*) from the direction of view (105°) that best displays the demarcation between the profiles of the 50S and 30S subunits. The representations were obtained with two different threshold levels; on the left with the same level as in (*A*) and on the right with a slightly higher level such that the location of the density minimum between the two subunits become visible. Bar, 10 nm.

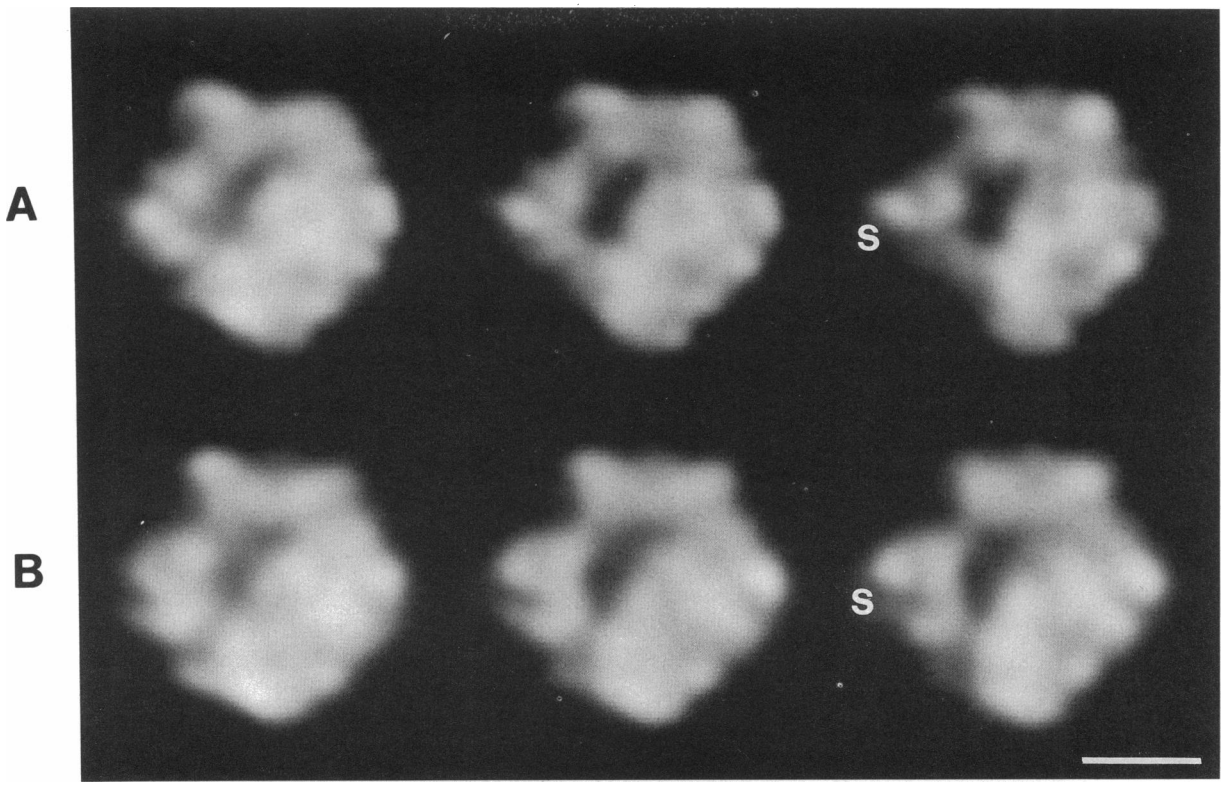

FIGURE 6 Conservation of the structure within the O-subrange of views. (*A*) Three central slices, parallel to the electron microscope support grid and spaced 1-nm apart, through the local 3D reconstruction obtained from views in the far-O region after rotation by 16° around the vertical (*y*) axis. (*B*) Equivalent slices through the local 3D reconstruction from the center-O region without rotation. *S*, the L7/L12 region. Bar, 10 nm.

ϕ, the tilt angle θ, and the rocking angle β of each projection were used to calculate equivalent angles in a unified coordinate system through the equations developed in Image Processing Methods. Since the object consisted of a set of hollow spheres with their centers situated in three different planes, the results are best displayed by slicing through the reconstruction along these planes.

The slices show (Fig. 7 *b*) that the degradation introduced by the 20° rocking is severe. After application of the multicone approach to these computer-simulated data, however (Fig. 7 *c*), it is evident that the artifacts have been virtually eliminated. As a future work, a method to calculate a 3D variance map from a set of 2D projections, using either the single-cone or the multicone technique, needs to be developed in order to quantify the decrease of variance achieved by application of the multicone strategy.

2.2 Results with the 70S monosome

In section 1, we showed that images in the far-O and center-O regions could be considered as being mainly rocking-related. A quantification of the rocking for each individual view could be obtained from the co-projections studies. Rocking angles were assigned to experimental views on the basis of the known angle of the most closely placed calculated projection in the co-projection map (see Fig. 2). In an effort to restrict the variability of our data set as much as possible to the rocking effect, we only used those experimental projections that were on the O-side of factor 1 (regions far-O and center-O) and that were, in addition, close to the actual pathway followed by the inactive projections. We made use of a map of factor 1 versus factor 5 to determine the region that was to be used in the multicone reconstruction. We defined in this map a rectangular region centered on the pathway of the co-projected calculated projections and whose width was one standard deviation of the variability along factor 5. The total number of particles that entered this multicone 3D reconstruction was 112, which is not much larger than the number used for any local reconstruction, since the constraint into a rectangle eliminated many peripheral projections.

We expected that this reconstruction would enhance those features that might have been degraded by the rocking behavior of the specimen in each of the local 3D

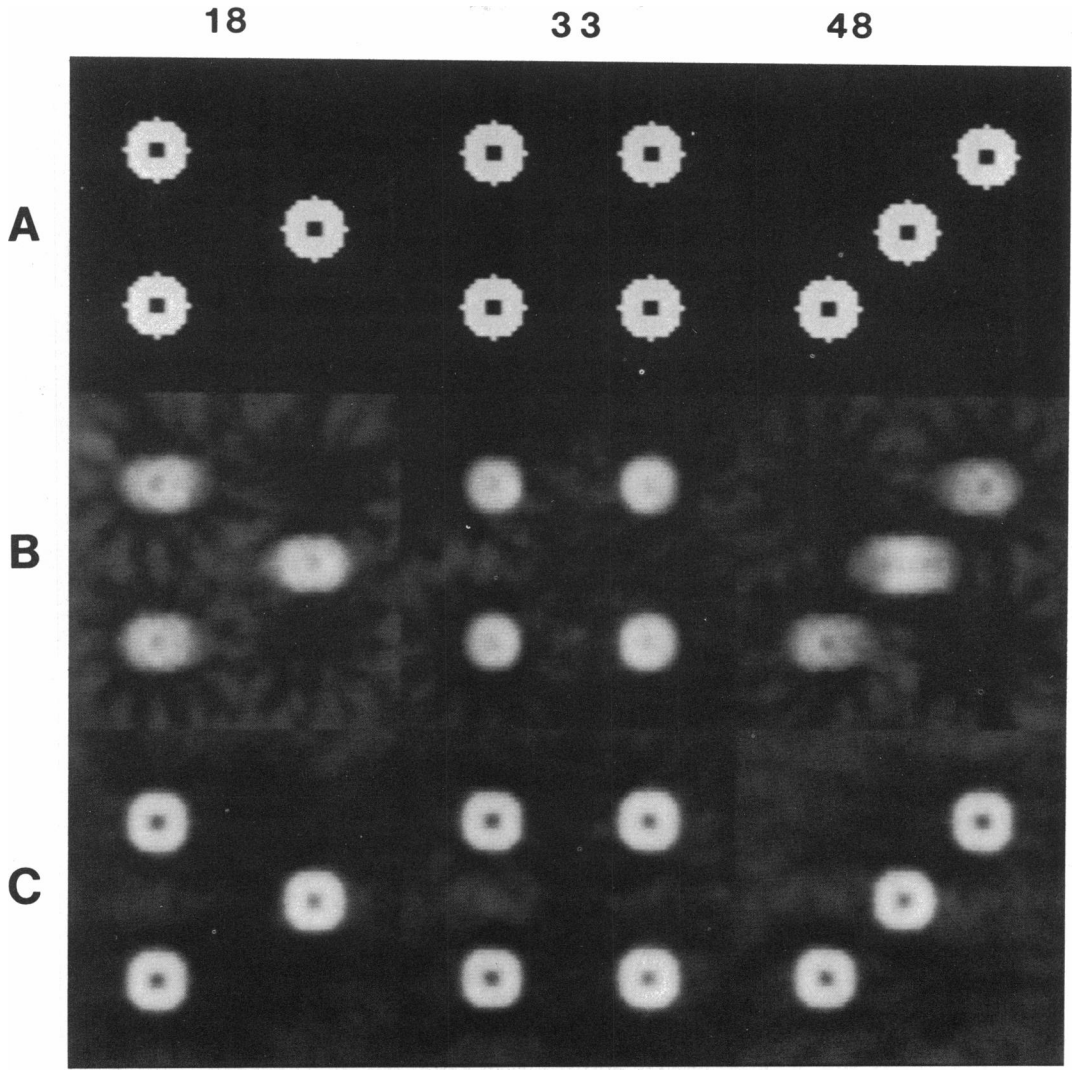

FIGURE 7 Slices through the 64 × 64 × 64 computer-generated test object used to study the behavior of the multicone 3D reconstruction method. The cutting plane was perpendicular to the z axis at levels z = 18, 33, and 48 (labeled, top of figure). The letters on the left refer to *A* the original object, *B* the object reconstructed without taking into account any rocking, and *C* the multicone 3D reconstruction.

reconstructions. However, the improvement should be less dramatic than in the computer-generated example since the estimated rocking range for each reconstruction was $\sim \pm 7°$, as opposed to $\pm 20°$ in the former case. On the other hand, the rectangular limitation has probably eliminated additional rocking effects about an axis perpendicular to the main rocking axis.

The 3D structure resulting from the application of the multicone technique (Fig. 8) will be referred to as the multicone reconstruction. We term "front" of the particle the side facing the exterior of the 30S subunit and "back" the one facing the exterior of the 50S subunit. This new reconstruction presents some interesting structural characteristics, such as the detailed substructure of the connections between the front and the back of the particle (Fig. 8 *B*), which is much better defined in this multicone reconstruction than in any of the local reconstructions (see companion paper by Wagenknecht et al., for further considerations). Also, the dimension along the x axis (that is running horizontal in Fig. 8) of the multicone reconstruction is slightly smaller (~10%) than for any local reconstruction.

DISCUSSION

We have addressed in this work the question of how the *E. coli* 70S monosome 3D structure, as determined from

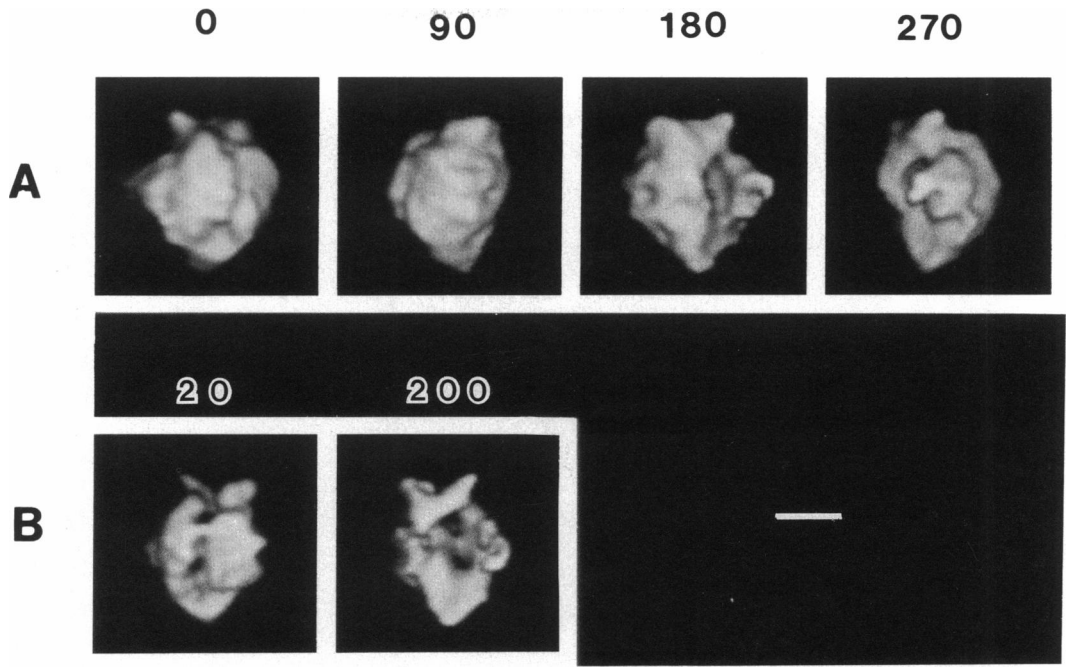

FIGURE 8 Surface representation of the multicone 3D reconstruction of the *E. coli* 70S monosome obtained from a portion of the images corresponding to the O-subrange of views. This reconstruction is presented in an orientation similar to the one of the center-O reconstruction (Fig. 5 *b*). The numbers on top of the figure represent the direction of view, 0°, 90°, 180°, and 270° for (*A*) and 20° and 200° for (*B*), in terms of a rotation around a vertical axis, from which the surfaces were calculated. (*A*) and (*B*) show the structure at two different threshold levels, the one used in (*B*) being higher in order to clearly show the pattern of connectivity from front to back described in the main test.

single-particle 3D reconstruction methods, depends on the orientation of the specimen on the electron microscopic support films. The *E. coli* 70S monosome in the O-R range of overlap views (Verschoor et al., 1986) has been the system considered in this study. The four local 3D reconstructions that we have calculated along the overlap range of views allow us to draw some conclusions about the extent of the heterogeneity of the 3D structure of the 70S monosome on the support films.

Behavior of the 70S monosome in the O-subrange of views

We have found that part of the O-R range, which we have termed the O-subrange, can be approximately explained by a rocking from $-35°$ to $\sim 0°$ of the 70S monosome on the support films with no substantial concomitant changes of the specimen structure. The rocking axis was found to virtually coincide with the one previously proposed by Verschoor et al. (1986) to explain the overlap range of views. The experimental evidence supporting this conclusion is very direct. The 3D reconstructions from the far-O and center-O regions can be best matched when the far-O reconstruction is rotated by 16° (Figs. 5 *A* and *B* and 6). This rotation also corresponds approximately to the relative rocking orientation between particles whose images lie in the centers of these two regions along factor one, as derived from the location of the calculated projections on the co-projected maps (Fig. 2). Since a rocking of the specimen on the support films was not found in previous structural studies of the *E. coli* 50S ribosomal subunit (Radermacher et al., 1987*a*, *b*; Carazo et al., 1988) under otherwise similar specimen preparation conditions to the ones used in this work, and since there exists no correlation between the location of the particles in the factorial maps and the micrograph from which they were extracted, we conclude that the rocking behavior is a characteristic of the 70S particle and is not caused by the support films.

While this rocking within the O-subrange of views is seen to conserve the general morphology of the monosome, there are some small, but noticeable, structural changes. A comparison of the 3D reconstructions from the far-O and center-O regions shows some differences mainly located at the interface between the 30S and 50S subunits. In particular, the far-O reconstruction is the single one in which some demarcation between the profiles of the 30S and the 50S subunit can be discerned (Fig. 5 *E*, 105° rotation, left and right). Also, very interestingly, there is a pronounced density minimum near the

interface between the two subunits at the location where the platform of the small subunit is supposed to be (Fig. 5 *E*, 105° rotation, right). Whether this minimum represents a physical separation between the two subunits, a positive staining of nucleic acids at the 30S subunit platform, or an actual indentation of the 30S at the platform is as yet difficult to decide on the basis of the present data (see companion paper by Wagenknecht et al., 1989).

Multicone 3D reconstruction

We have introduced a new methodology, which we call the multicone 3D reconstruction method, that allows the orientation changes due to rocking to be taken into account, provided that the rocking angles and axis are known, and provided that the specimen structure does not change during the course of the rocking.

The study performed on a computer-generated object showed that, not surprisingly, a modeled rocking of the specimen on the support film could introduce severe distortions in the 3D reconstruction (compare Figs. 7 *A* and *B*), and we were able to demonstrate that our generalized multicone 3D reconstruction technique could correct for the rocking behavior of the specimen (Fig. 7 *C*). In fact, this approach has an additional advantage over the single-cone method, in that it exploits the increase in effective tilt (measured relative to the direction of the electron beam) available through the rocking. Thus the amount of missing-cone data (cf. Hoppe and Hegerl, 1980) that is always associated with a limited-tilt data-collection geometry is reduced, and the quality of the reconstruction is improved. For example, for a projection image computed with a rocking angle of 20° the ϕ and θ angles in the 20° data cone are $\phi = 20°, \theta = 50°$, the new ϕ' and θ' in the coordinate system of the 0° degree (reference) data cone are $\phi' = 16.3$ and $\theta' = 69$; the effective tilt is thus increased from 50° to 69°.

The most important new feature of the multicone 3D reconstruction calculated from views of the 70S monosome in the O-subrange is the improved definition of the connections between the front and the back of the 50S subunit within the 70S particle (Fig. 8 *B*). It is important to note here that these connections have been consistently found by Radermacher et al. (1987*b*) and by Carazo et al. (1988) in several 3D reconstructions *E. coli* 50S subunits. However, in the case of the 70S monosome it was necessary to obtain the multicone 3D reconstruction in order to visualize these features almost as clearly as in the studies of the 50S subunit (see Wagenknecht et al., companion paper, for further considerations). The dimensions the directions perpendicular to the rocking axis are also ~10% smaller in the multicone reconstruction than in any of the local reconstructions, most probably because the blurring produced by the small amount of rocking still affecting each local reconstruction has now been entirely eliminated.

An important caveat applies to this 3D reconstruction: the previously described differences between the structures from the far-O and center-O regions may introduce some degradations in the multicone reconstruction. We must assume that particles lying in the range between far-O and center-O are gradually changing appearance between the two local reconstructions obtained from those regions. This implies that when views from all particles are combined to calculate a single 3D reconstruction, the areas in which they differ are visualized as blurred features, whereas the areas that are most conserved come out as sharper, better defined structures.

Behavior of the 70S monosome in the R subrange of views

The other part of the O-R range of views, that is the R subrange, comes from a specimen that has apparently interacted with the support film in a different way, resulting either in a further rocking accompanied by some structural modifications of the specimen structure (center-R region), or in a totally different pattern of rocking (far-R region) around an axis approximately perpendicular to the one previously identified.

The center-R reconstruction is still very similar, in many features, to the local reconstruction from the O-subrange. A likely explanation for the failure to co-project the calculated projections along factor 1 in the region of the center-O views (i.e., the failure to explain the corresponding experimental projections in terms of our global model under the assumption that factor 1 is entirely rocking-related) consists in some conformational changes in the monosome structure (as described in Results) that can interfere with the co-projection analysis, which is suitable only to detect rotations of essentially unchanged structures. Another possible explanation could be a less straightforward relationship between factors and physical effects (such as rocking) than previously supposed (Verschoor et al., 1986).

On the other hand, the local far-R 3D reconstruction (Fig. 5 *D*) shows an apparent resolution that is much lower than any other reconstruction. Since the number of particles is similar to that in the other reconstructions, this effect is not related to the statistical resolution limitation, and it probably reflects a higher local (i.e., in factor space) heterogeneity of the particle population. A second rocking effect around an axis essentially perpendicular to the one relating the other three reconstructions is also evident, probably playing an important role in the local heterogeneity.

General considerations on the structural models of the 70S monosome

Previous models of the ribosome structure derived from electron microscopy were obtained by a more or less subjective interpretation of the relationship between different views of the monosome and ribosomal subunits (for a review see Wittmann, 1983). These models attempted to reconcile the different views in terms of changes in the orientation of the specimen with respect to the supporting films. Although the possibility that the ribosome might be affected by a distortion in each of the different views has always been a concern, there existed no quantitative way to assess the magnitude of these effects. The introduction of single-particle 3D reconstruction methods has changed this situation completely, making it possible to obtain the structure of the ribosome separately and independently in each orientation that produces one of these views. Since data are not merged unless it can be proved that they arise from basically the same particle structure, there is no necessity for a priori assumptions relating particles in different views.

In this study of the overlap range of views of the 70S monosome we have shown that the 3D structure of the ribosome changes between the O-view and the R-view, but that these changes are of a relatively small scale. This is in agreement with some previous results on the general behavior of ribosomes on supporting carbon films (Kellenberger et al., 1982). We were able to prove that, within part of this overlap range, the ribosome behaves approximately like a rigid body that assumes different rocking positions on the supporting carbon films.

On the other hand, none of these reconstructions presents a clear separation between the two ribosomal subunits. Furthermore, we were unable to reproduce the L view (Lake, 1976; Verschoor et al., 1986) from our reconstructions by tilting the structure further and projecting it. The L view is usually interpreted as a nonoverlap view of the ribosome presenting the two subunits separated and roughly side-by-side (corresponding approximately to the 90°/270° views shown in Fig. 8). Other 3D studies also show a clear separation between the subunits, such as the crystalline 3D reconstruction of the *Bacillus stearothermophilus* 70S monosome presented by Arad et al. (1987), and the single-particle 3D reconstruction of the 80S monosome from rabbit reticulocytes obtained by A. Verschoor and J. Frank (manuscript submitted for publication), which was based on a view that appears to be closely related to the L view of the 70S monosome. These facts lead us to believe that there are significant differences between the morphology that the monosome assumes in the O-R range of overlap views and the morphology in the nonoverlap L view. Thus, further systematic studies using views other than those presented in this work will be necessary to reach a more precise model of the ribosome structure.

CONCLUSIONS

Using the O-R range of overlap views of the *E. coli* 70S monosome as a model system we have investigated in what manner the 3D structure of isolated specimens can change, depending on the way they interact with the support films. We have shown that precise assessments of the structural heterogeneities resulting from the different types of specimen/support interaction can be obtained using MSA and local 3D reconstructions. Thus, a methodology to study the structural interactions between the specimen and the support films has been provided. Furthermore, the multicone 3D reconstruction method has been proved to be effective in compensating for a rigid-body rocking of the specimen on the films.

Regarding the 3D structure of the *E. coli* 70S monosome, we have obtained the important result that many structural characteristics are very well preserved along the O-R range of overlap views. Particularly important features are the mutual orientations of the 50S and 30S ribosomal subunits (as deduced for their external profiles), the presence of an accessible interface canyon, and of apparent channels between the front and the back of the 50S subunit. Because these structural characteristics are conserved, they provide a reliable structural framework that allows functional relationships to be tested or hypothesized (see companion paper by Wagenknecht et al., 1989).

We thank Adriana Verschoor for discussions and Bob Grassucci for technical assistance.

This work was supported in part by National Institutes of Health grant 1R01 GM29169 and National Science Foundation grant 8313405.

Received for publication 15 July 1988 and in final form 26 October 1988.

REFERENCES

Arad, T., J. Piefke, S. Weinstein, H. -S. Gewitz, A. Yonath, and H. G. Wittmann. 1987. Three-dimensional image reconstruction from ordered arrays of 70S ribosomes. *Biochimie.* 69:1001–1006.

Bretaudiere, J. P., and J. Frank. 1986. Reconstitution of molecular images analyzed by correspondence analysis: a tool for structural interpretation. *J. Microsc.* 144:1–14.

Carazo, J. M., and J. Frank. 1988. Three-dimensional matching of macromolecular structures obtained from electron microscopy: an

application to the 70S and 50S *E. coli* ribosomal particles. *Ultramicroscopy.* 25:13–22.

Carazo J. M., T. Wagenknecht, M. Radermacher, V. Mandiyan, M. Boublik, and J. Frank. 1988. Three-dimensional structure of 50S *E. coli* ribosomal subunits depleted of proteins L7/L12. *J. Mol. Biol.* 201:393–404

Crowther, R. A., D. J. DeRosier, and A. Klug. 1970. The reconstruction of a three-dimensional structure from projections and its application to electron microscopy. *Proc. R. Soc. Lond. B. Biol.* A317:319–340.

Eccles, F. M., E. P. Vance, and T. M. Mikula. 1982. Analytic and Vector Geometry. Addison-Wesley, Menlo Park, CA.

Frank, J., and M. van Heel. 1982. Correspondence analysis of aligned images of biological particles. *J. Mol. Biol.* 161:124–137.

Frank, J., W. Goldfarb, D. Eisenberg, and T. S. Baker. 1978. Reconstruction of glutamine synthetase using computer averaging. *Ultramicroscopy.* 3:283–290.

Frank, J., A. Verschoor, and M. Boublik. 1981. Computer averaging of 40S ribosomal subunits. *Science (Wash. DC).* 214:1353–1355.

Frank, J., A. Verschoor, and T. Wagenknecht. 1985. Computer processing of electron microscopic images of single particles. *In* New Methodologies in Studies of Protein Configuration. T. T. Wu, editor. van Nostrand Reinhold, New York. 36–89.

Frank, J., J. P. Bretaudier, J. M. Carazo, A. Verschoor, and T. Wagenknecht. 1988*a*. Classification of images of biomolecular assemblies: a study of ribosomes and ribosomal subunits of *Escherichia coli. J. Microsc.* 146:113–136.

Frank, J., J. M. Carazo, and M. Radermacher. 1988*b*. Refinement of the random-conical reconstruction technique using multivariate statistical analysis (MSA) and classification. *Eur. J. Cell Biol.* in press.

Henderson, R., and P. N. T. Unwin. 1975. Three-dimensional model of purple membrane obtained by electron microscopy. *Nature (Lond.)* 257:28–32.

Hoppe, W. and R. Hegerl. 1980. Three-dimensional structure determination by electron microscopy. *In* Computer Processing of Electron Microscopy Images. Springer-Verlag, New York.

Kellenberger, E., M. Haner, and M. Wurtz. 1982. The wrapping phenomenon in air-dried and negatively stained preparations. *Ultramicroscopy.* 9:139–150.

Lake, J.A. 1976. Ribosome structure determined by electron microscopy of *Escherichia coli* small subunits, large subunits and monomeric microsomes. *J. Mol. Biol.* 105:131–159.

Provencher, S. W., and R. H. Vogel. 1983. Regularization techniques for inverse problems in molecular biology. *In* Numerical Treatment of Inverse Problems in Differential and Integral Equations. P. Deuflhard and E. Hairer, editor. Proceedings of an International Workshop, Heidelberg. Aug. 30–Sept. 3, 1982, Birkhaeuser Verlag, Boston.

Radermacher, M. 1980. Dreidimensionale Rekonstruktion bei Kegelförmiger Kippung im Elektronenmikroskop. Ph.D. Thesis, Technische Universität München.

Radermacher, M. 1988. Three-dimensional reconstruction of single particles from random and nonrandom tilt series. *J. Electron Microsc. Tech.*9:359–394.

Radermacher, M., and J. Frank. 1984. Representation of three-dimensionally reconstructed objects in electron microscopy by surfaces of equal density. *J. Microsc.* 135:77–85.

Radermacher, M., T. Wagenknecht, A. Verschoor, and J. Frank. 1987*a*. Three-dimensional reconstruction from a single-exposure random conical tilt series applied to the 50S ribosomal subunit of *E. coli. J. Microsc.* 146:113–136.

Radermacher, M., T. Wagenknecht, A. Verschoor, and J. Frank. 1987*b*. Three-dimensional structure of the large subunit from *Escherichia coli. EMBO (Eur. Mol. Biol. Organ. J.)* 6:1107–1114.

Vainshtein, B. K., and A. B. Goncharov. 1986. Determination of the spatial orientation of arbitrarily arranged identical particles of an unknown structure from their projections. *Proc. XIth Congr.* on Electron Microscopy. Kyoto, Japan. 459–460.

van Heel, M. 1987. Angular reconstitution: a posteriori assignment of projection directions for 3D reconstruction. *Ultramicroscopy.* 211:111–124.

van Heel, M., and J. Frank. 1981. Use of multivariate statistics in analysing the images of biological macromolecules. *Ultramicroscopy.* 6:187–194.

Verschoor, A., J. Frank, T. Wagenknecht, and M. Boublik. 1986. Computer-averaged views of the 70S monosome from *Escherichia coli. J. Mol. Biol.* 187:581–590.

Wagenknecht, T., J. M. Carazo, M. Radermacher, and J. Frank. 1989. Three-dimensional reconstruction of the ribosome from *Escherichia coli. Biophys. J.* 55:00–00.

Wittmann, H. G. 1983. Architecture of prokaryotic ribosomes. *Annu. Rev. Biochem.* 52:35–65.

Zhang, N. -Y., T. Wagenknecht, M. Radermacher, T. Obrig. and J. Frank. 1987. Three-dimensional reconstruction of the 40S ribosomal subunit from rabbit recitulocytes. *Proc 45th Meeting of the EMSA.* San Francisco, CA 936–937.